2.A.1 *Nuclear Physics* A93 (1967) 648—672; © *North-Holland Publishing Co., Amsterdam*

(p, n) and (p, 2n) CROSS SECTIONS OF NINE ELEMENTS BETWEEN 7.0 AND 15.0 MeV

G. CHODIL, R. C. JOPSON, HANS MARK, C. D. SWIFT, R. G. THOMAS and M. K. YATES †

University of California, Lawrence Radiation Laboratory ††, *Livermore, California*
and
University of California, Department of Nuclear Engineering, Berkeley, California

Received 31 October 1966

Abstract: The excitation functions and absolute cross sections for (p, n) and (p, 2n) reactions were measured for thin targets of the elements aluminium, titanium, vanadium, cobalt, zirconium, niobium, silver, tantalum and gold. The energy of the incident proton beam was varied between 7.0 and 15.0 MeV. The emitted neutrons were detected by a large gadolinium-loaded, liquid scintillator detector, and the two competing processes were separated by a statistical analysis. Thick target total neutron yield cross sections were also measured. New nuclear level-density parameters for these elements were determined from the results.

E NUCLEAR REACTIONS Al(p, n); Ti, V, Co, Zr, Nb, Ag, Ta, Au(p, n), (p, 2n), E=7–15 MeV; measured $\sigma(E)$. ^{51}V, ^{59}Co, ^{93}Nb, ^{181}Ta, ^{197}Au deduced nuclear level density. Natural targets.

1. Introduction

The (p, n) cross sections have been studied extensively in recent years, but there is much less information available on the (p, 2n) reaction. The reasons for this lack of information stem mainly from the difficulties encountered in activation analysis which is the experimental method most frequently used [1–9]). Activation analysis puts three restrictions on the reaction studied: (i) the end product must be unstable; (ii) the half-life of the end product must be long enough to permit accurate counting techniques to be used; and (iii) the relevant decay scheme must be well known. In most (p, n) reaction all of these citeria are met; however, in many (p, 2n) reactions at least one of them is violated. In the heavier elements the final product of a (p, 2n) reaction is often stable; e.g., ^{107}Ag(p, 2n)^{106}Cd, ^{181}Ta(p, 2n)^{180}W and ^{197}Au(p, 2n)^{196}Hg. In the lighter elements the half-life of the product is often very short; e.g., ^{27}Al(p, 2n)^{26}Si (2 sec) and ^{31}P(p, 2n)^{30}S(1.4 sec). In addition, decay schemes for many product isotopes are not well established.

† Submitted in partial fulfillment of the requirements for the Ph.D. in Engineering Science, Department of Nuclear Engineering, University of California, Berkeley, California.

†† Work performed under the auspices of the U.S. Atomic Energy Commission.

The present method, based on detecting the emitted neutrons, circumvents these difficulties. Other experimenters have been using "long counters" as the neutron detector [10]). However, for the measurement of absolute cross sections and excitation functions, large liquid scintillation detectors have certain advantages.

Large liquid scintillators were originally developed at Los Alamos and have been used by several groups for the measurement of $\bar{\nu}$, the average number of neutrons emitted in fission [11]). More recently, large scintillators have been employed to determine (n, 2n) cross sections [12]).

The experiment was performed on the Livermore variable-energy cyclotron, and the results are presented in tabular and graphical form. The (p, 2n) reactions were measured in all elements except aluminium, in which no (p, 2n) reaction was detected in the energy range considered here. A search for a (p, 3n) reaction was conducted for the two heavy elements, tantalum and gold, but none was found below 15 MeV.

2. Physical arrangement

The scintillator tank was located in a cave especially built for it outside the UCLRL-Livermore cyclotron target pit (fig. 1). The complete layout of the magnet, beam pipe and collimator arrangement is shown in fig. 1. The beam was electrostatically deflected from its orbit in the cyclotron magnet, brought through a quadrupole lens and a steering magnet and then periodically deflected into collimator slits by sweeper plates. It was then brought outside the target pit and through the centre of the scintillator tank.

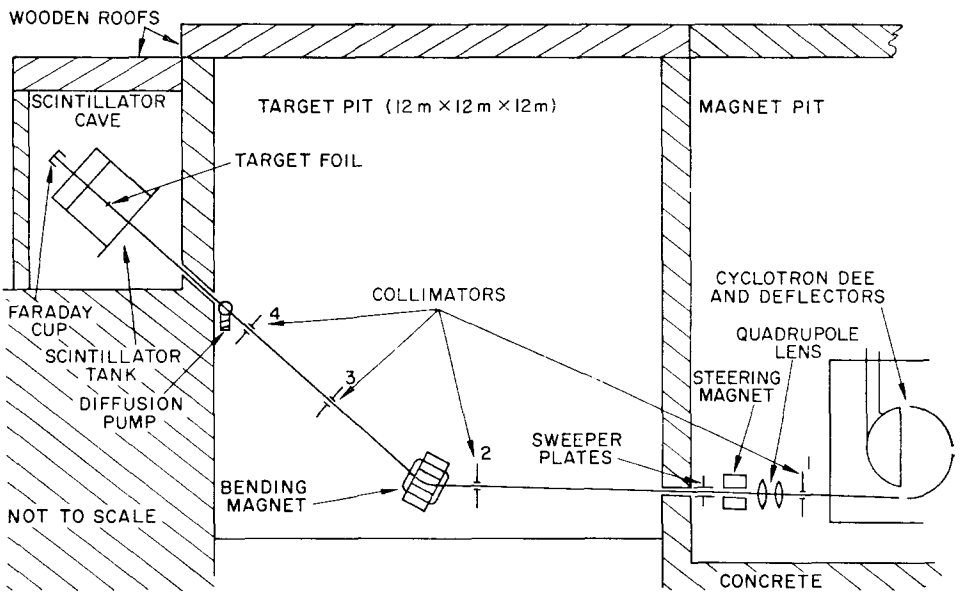

Fig. 1. Beam geometry. Cyclotron is in the pit at right, beam transport system is in the centre pit, and liquid scintillator is in the shielded cave on the left side of the drawing.

The system was lined up visually to ± 0.16 cm with a transit mounted behind the scintillator tank at the beginning of each run. In addition, the beam was centred on the foil by focussing it through a 2 cm collimator temporarily put in the foil position. The target foil size was 4 cm in diam. The cross section of the beam at the target was generally about 0.6×1.3 cm when completely collimated.

The cyclotron frequency was varied from 7 to 9×10^6 cycles/sec, that is, 110 to 140 nsec between cyclotron beam pulses. Since the mean time to capture in the scintillating solution is approximately 20 μsec, it was nesessary to sweep the proton beam at a frequency slow enough so that the slowing down and capture process of neutrons produced by different proton pulses did not overlap. This beam sweeping was accomplished with an electrostatic sweeper system which operated at 2×10^3 cycles/sec. The width of the swept beam pulse was about 0.35 μsec and contained between two and three cyclotron beam pulses. The sweeper plates were synchronized with the rf system, and a pulse from this system was used as the trigger for the counting electronics.

Neutron and gamma-ray background from the collimators was minimized by facing the collimator jaws with graphite and stacking paraffin wax around the No. 2 collimator. (Over 99 % of the beam was stopped at that point.)

3. Current monitors

After passing through the target foil, the proton beam went through a transmission ion chamber and was stopped in a Faraday cup (fig. 2). The ion chamber consisted

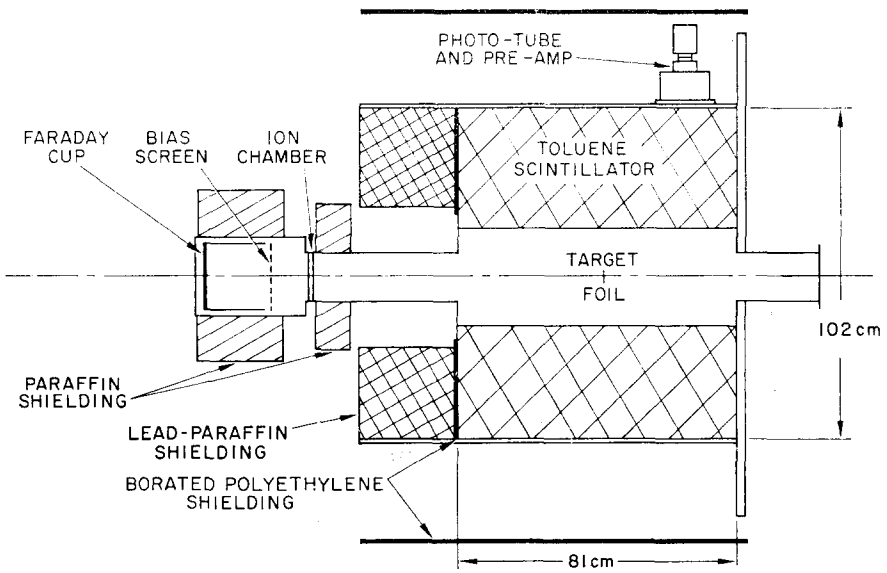

Fig. 2. Liquid scintillator tank. Ion chamber monitor and Faraday cup are shown in the left side of the picture.

of two parallel 25 μm aluminium foils 1.3 cm apart. Helium was used as the filling gas for this chamber and was kept at an absolute pressure of 50 mm Hg. The exit foil was grounded and the entrance foil was kept at +200 V and connected to a Tennelec low-noise preamplifier. The ion chamber output was proportional to the number of protons per beam pulse N_p and was assumed to be a linear function of N_p. The varia-

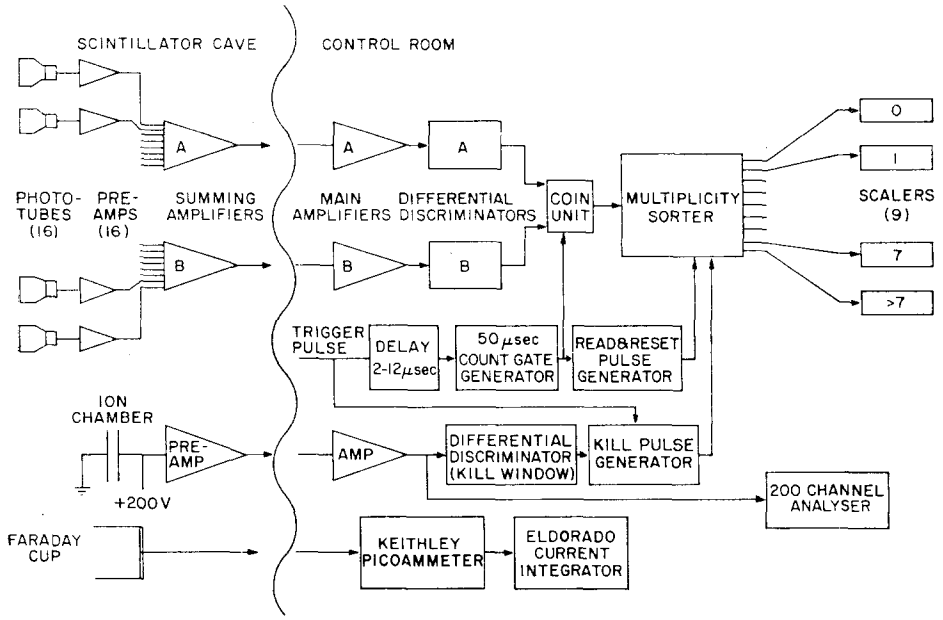

Fig. 3a. Block diagram of the electronics system.

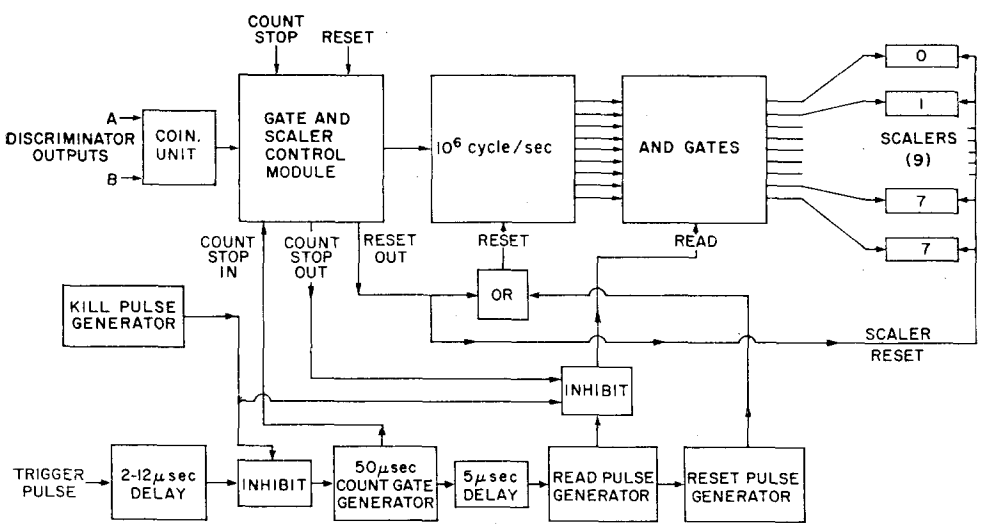

Fig. 3b. Detail of the multiplicity sorting system.

tion of pulse height with respect to N_p was measured and the linearity was found to be within $\pm 5\,\%$ over most of the spectrum. The pulse-height output was recorded on a 200-channel analyser.

The ion chamber output was used to operate a circuit (designated as the kill system) which prevented recording of the information from those gates whose initial beam pulse size fell outside certain limits (outside the kill window). The kill pulse was generated when a pulse from the ion chamber, after amplification, fell outside the window of a differential discriminator. (See block diagram of electronics in fig. 3.) The calibration of the ion chamber and kill window is described in sect. 8.

The Faraday cup was made of tantalum and had a graphite beam stop. A bias screen kept at -300 V potential was used to suppress secondary electrons from the cup and primary electrons produced on the exit foil of the ion chamber. The beam current was collected in the cup and fed into a Keithley Model 410 picoammeter. Instantaneous current was read from this meter for beam monitoring and tune-up purposes. The recorder output from the meter was converted into a current and integrated in an Eldorado Model CI-100 current integrator. The system was calibrated with a Beckman current source using calibration currents of around 10^{-11} A, since these were the normal proton beam currents used.

4. Target foils

The target foils used were discs 4 cm in diam, with thicknesses around 3 mg/cm^2, except Al (4.6 mg/cm^2) and Au (2.0 mg/cm^2). This particular thickness was chosen as a compromise between two requirements (i) that the foils be thin enough so that proton multiple scattering be minimized and (ii) that the foils be thick enough to be used without backings and strong enough to survive repeating handling. Requirement (i) proved to be the more stringent of the two. After making the ion chamber as large as practical (15 cm diam) and moving the ion chamber and Faraday cup close to the scintillator tank, it was found that less than 0.2 % of the beam was scattered outside the ion chamber at 7 MeV with any foil. Energy loss for a 10 MeV proton was less than 0.1 MeV in all foils except aluminium, in which it was 0.15 MeV.

All foils except aluminium, silver and gold were furnished by the Oak Ridge National Laboratory. The other three foils were supplied by M. Williamson of Lawrence Radiation Laboratory, Livermore. The average thickness of each foil was measured by carefully weighing the foil and measuring the area. In addition, the relative uniformity of each was checked by measuring the energy loss of mono-energetic α-particles passing through the foil.

5. Scintillator tank

The scintillator tank has been described in an earlier report [12]). It was modified slightly for this experiment (fig. 2). First, the chamber was shortened to 81 cm in

length, and second, a through tube 30 cm in diam was installed in the centre of the tank to make possible a six-position foil holder which was driven remotely and could be positioned at any point in the chamber.

Sixteen Dumont No. 6364 photomultiplier tubes 13 cm in diam were placed symmetrically around the chamber. They were mounted on glass viewing ports with a colourless potting compound (General Electric LTV 502 Clear Silicone Potting Compound). The inside of the chamber was painted with a white, diffuse reflecting paint (Plastite Paint No. 7122-H, Wisconsin Protective Coating Corporation) to aid reflection of photons into the photocathodes, which covered only 6 % of the surface area. The chamber was filled with 700 l of toluene (C_7H_8) mixed with 5 g/l p-terphenyl, 0.1 g/l POPOP and 10 g/l gadolinium octoate. The solution was bubbled with nitrogen before it was pumped into the tank and the system was kept under a positive overpressure of 100 mm Hg of nitrogen pressure to avoid oxygen pick-up and the quenching associated with it [13]).

Although the chamber was located in its own especially built cave extra shielding was added; 1.3 cm thick borated polyethylene sheets were put around the outside of the chamber to prevent thermal neutrons from entering the chamber, and the rear of the chamber was shielded with paraffin and lead-paraffin to prevent neutrons from the ion chamber - Faraday cup region from entering.

Neutrons produced by the proton beam striking the target in the centre of the detector entered the liquid and were slowed down, primarily by collisions with the hydrogen in the solution and were either captured in the gadolinium (gadolinium: hydrogen capture ratio 20:1) or leaked out of the chamber. The (n, γ) reaction in gadolinium produces 8–9 MeV of gamma-ray energy, usually shared among several gamma rays. Some of these underwent Compton scattering in the liquid, and the resulting recoil electrons produced the scintillations which were then detected by the photomultiplier system.

6. Electronics

A block diagram of the electronics is shown in fig. 3. The 16 photomultiplier tubes were split into two banks which were arranged so that each bank viewed the entire chamber. Each phototube had its own transistorised charge-sensitive preamplifier. The gains of all photomultiplier tube-preamplifier units were set equal by using a neutron source placed in the centre of the chamber. The preamplifier outputs were then fed into two transistorised, operational-type, summing amplifiers. Signals from the summing amplifiers were brought into the cyclotron control room by about 30 m of shielded cable. These signals were then amplified in a pair of transistor amplifiers which had a maximum gain of 1000 and double *RC* differentiation shaping with *RC* time constants of 0.1 μsec. The amplified signals then were fed into two differential discriminators which excluded small pulses from natural background, tube noise and large pulses produced by cosmic radiation.

The pulse used to actuate the proton beam sweeper plates also triggered an electronic gate which opened and allowed the scalers to count the neutrons produced by that beam pulse. This gate was left open for 50 μsec to allow capture of over 90 % of the neutrons it was delayed 2 μsec with respect to the beam to prevent detection of signals coming from prompt gamma radiation from the target or beam stop, or recoil protons produced during the neutron slowing-down process. A triple coincidence made with the two signals and the 50 μsec gate tended to reduce the effect of photomultiplier and amplifier noise pulses. During the 50 μsec gate, a scalar counted the number n of pulses from the coincidence unit. At the end of the gate, if there was no kill pulse, a count was recorded on the nth scaler ($n = 0, 1, 2 \ldots 7, > 7$); if a kill pulse occurred, the count was discarded.

7. Detector efficiency

The detector efficiency was determined by using a source of ^{252}Cf, a nucleide that fissions spontaneously. The source was mounted on a solid-state detector and was placed in the centre of the scintillator tank. The output of the silicon-barrier detector was amplified by a Tennelec low-noise preamplifier and then fed into a bias level which was set to exclude the alpha events. Only 2 μsec after a pulse corresponding to a fission fragment was detected the count gate was opened; it remained open for the usual 50 μsec interval. The kill window excluded those gates in which two fissions occurred. Two runs were made, one with source in the chamber and one with the source removed.

After the usual correction for counting losses in the electronics and the subtraction of background (see sect. 8), the probability per fission for neutron detection P was calculated. Then, taking $\bar{\nu}$ for ^{252}Cf to be 3.782 (ref. [11])), the detector efficiency E was given by $E = P/3.782$. The average efficiency during our runs was 60 %. No attempt was made to correct this efficiency for neutron energy.

8. Data analysis

The procedure followed in analysing the data was similar to that employed by previous workers in the field. The essential idea is that, if only (p, n) processes were present, then the counts in the n channels would be distributed according to a Poisson distribution. If (p, 2n) reactions can occur, then the Poisson distribution will not be observed. The observed deviations from the Poisson distribution can be used to infer the magnitude of the (p, 2n) cross section.

As stated earlier, the cyclotron beam was swept onto the target at frequencies around 2×10^3 cycles/sec. Each time the beam was swept across the target, a pulse from the sweeping system triggered the 50 μsec count gate. The number n of neutrons or background events observed during each count gate was recorded on the appropriate nth scaler.

The following definitions for each scaler ($n = 0, 1, 2, \ldots$) were employed:
F_n was the probability/gate of *detecting n events* in the scintillator due to signal plus background and
B_n the probability/gate of *detecting n events* in the scintillator due to background alone.
After removing the effect of background events,
D_n is the probability/gate of *detecting n* neutrons (from the foil).
After correcting for detector efficiency, we had
P_n is the probability/gate of *producing n* neutrons (from the foil).
Also, E was defined as the detector efficiency; C_f as the total number of signal + background gates, C_b the total number of background gates and k the probability that any two events occurring during a gate would be unresolved by the counting system.

After runs both with the foil in place and with a blank foil holder in place, the numbers on the scalers were divided by C_f and C_b to obtain F_n' and B_n', respectively. (The primes on these quantities mean that no correction for counting losses has been made.) Finally, the probabilities were corrected for counting losses.

Counting losses due to "pile-up" arose because there was a finite probability that two or more events would occur within a time which was shorter than the combined resolving time τ of the system and amplifiers and scalers. The probability k that two events occurred within $\pm\tau$ of each other is, for neutrons produced at $t = 0$, equal to

$$k_f = 2\tau \int_2^{52} [f(t)]^2 \, dt, \tag{1}$$

where $f(t)$ is the normalized capture rate versus time spectrum (fig. 4). The quantity k_f was calculated and found to be equal to 0.016 ± 0.002 for a measured value of τ of 0.25 μsec. For completely random background events,

$$k_b = \frac{2\tau}{50 \ \mu\text{sec}} = 0.010.$$

In the present experiment, a combination of neutrons produced at $t = 0$, together with a random background, was observed. Therefore, k was set as a function of the ratio of counts produced by neutrons to counts produced by neutrons plus random events. If this ratio is a, then

$$k = 0.50(0.012a^2 + 0.02). \tag{2}$$

Since the probability that two events were unresolved turned out to vary from 0.010 to 0.016, higher-order effects were neglected.

Now if n events occurred, the probability that that gate would be recorded on the $(n-1)$st scaler was $\binom{n}{2}k$ where $\binom{n}{1}$ was the familar binomial coefficient $n!/i!(n-i)!$. Therefore,

$$F_n' = F_n - \frac{n!}{2!(n-2)!} kF_n + \frac{(n+1)!}{2!(n-1)!} kF_{n+1}. \tag{3}$$

Similar equations hold for the background (B_n', B_n) and these expressions were solved for F_n and B_n for $n = 1, 2, 3 \ldots$.

The quantities D_n were calculated by inverting the following relationships:

$$F_n = D_nB_0 + D_{n-1}B_1 + \ldots + D_0B_n, \qquad n = 0, 1, 2 \ldots. \tag{4}$$

The probabilities P_n were calculated from the following equations

$$P_n = \sum_{i=n} \binom{i}{n} \frac{1}{E^i} (E-1)^{i-n} D_i, \qquad n = 0, 1, 2, \ldots. \tag{5}$$

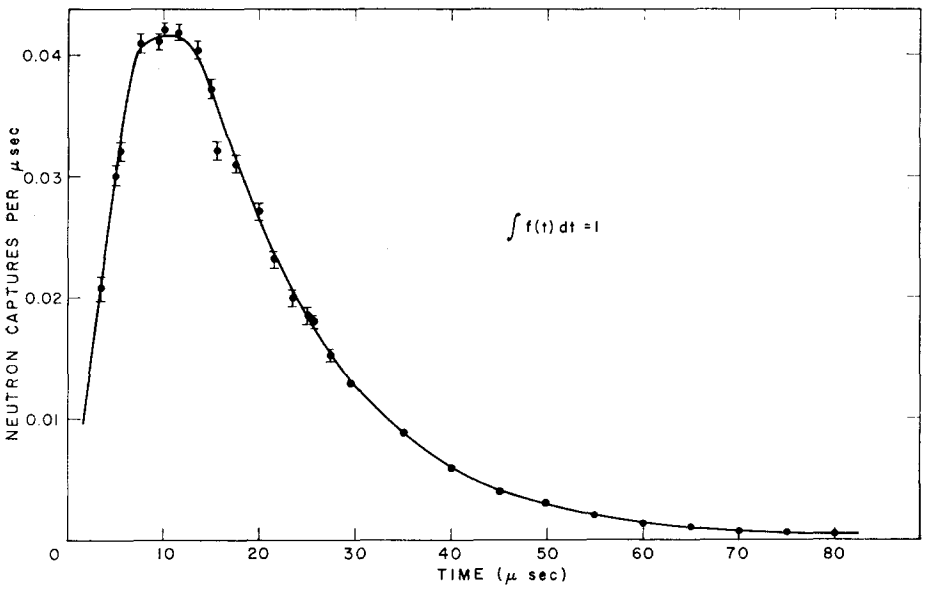

Fig. 4. Capture rate of neutrons in the scintillator tank as a function of time after the beam pulse for the gadolinium-loaded toluene.

The cross sections were computed from these relations

$$\begin{aligned} P_0 &= e^{-x}e^{-y}, \\ P_1 &= xe^{-x}e^{-y}, \\ P_2 &= \frac{x^2}{2!} e^{-x}e^{-y} + ye^{-x}e^{-y}, \\ P_3 &= \frac{x^3}{3!} e^{-x}e^{-y} + xye^{-x}e^{-y}, \\ P_4 &= \text{etc.} \end{aligned} \tag{6}$$

Where the Poisson distribution has been assumed applicable, and where

$$x = N_pNt\sigma(\text{p, n}), \qquad y = N_pNt\sigma(\text{p, 2n}), \tag{7}$$

N_p is the number of protons per pulse, N the nuclear density of targets in atoms/cm^3 and t the target thickness in cm.

All but two of the eqs. (6) are redundant. Theoretically any two of the equations could have been chosen to be solved simultaneously; however, only the second and third equations were useful because of the limitations imposed by counting statistics.

These two equations could have been easily solved if there had not been a compli-

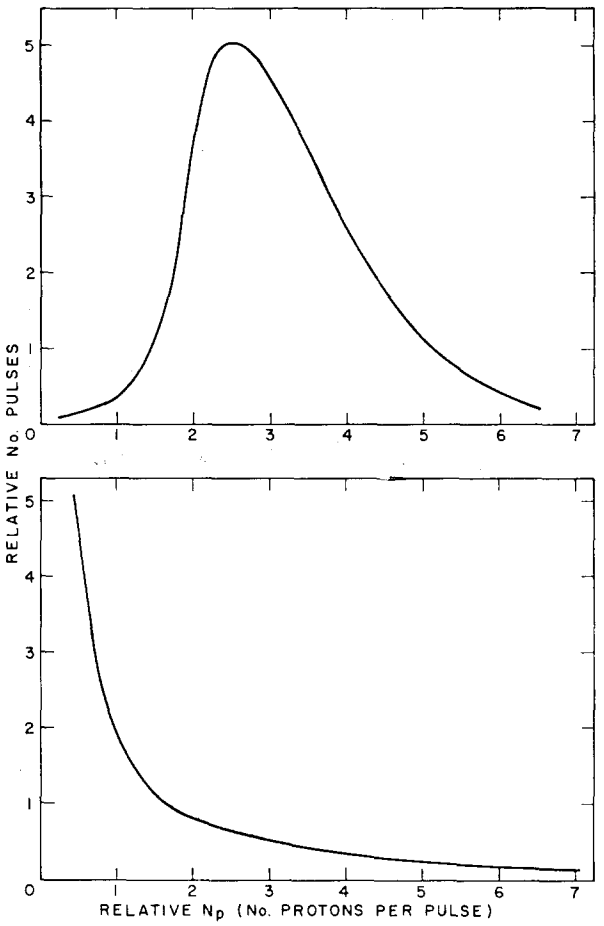

Fig. 5. Typical beam pulse intensity distribution as measured by the ion chamber.

cating feature of the proton beam. The foregoing analysis tacitly assumed that there were no pulse-to-pulse variations in the beam intensity, i.e. N_p was assumed constant. However, this was not the case; the output of the ion chamber varied considerably, as is evidenced by the two typical spectra from it shown in fig. 5. Since the number of protons per gate varied widely, this effect had to be incorporated into the analysis. In general, this required that all terms in the above equations be replaced with the

appropriate average quantities, where the averaging was over the ion chamber spectrum. This procedure led to the functional relationship

$$\overline{D_n} = \overline{f(F_i, B_j)}. \tag{8}$$

But, in order to analyse the data in terms of measured quantities, the following relationship must be obtained:

$$\overline{D_n} = f(\bar{F}_i, \bar{B}_j). \tag{9}$$

For this relationship to hold it was necessary that the background spectrum be independent of the number of protons per pulse N_p.

To circumvent this difficulty, the kill circuitry was used to select a certain part of the ion chamber spectrum. Theoretically, the kill window could have been set narrow enough so that the approximation that N_p was a constant would have been valid. However, doing this would have made it necessary to discard better than 95 % of the beam gates and would have made it difficult to determine with accuracy the fraction of the proton beam in the kill window. Therefore, a window wide enough to accept from 20 to 30 % of the gates was chosen. In a window of this size it was assumed that eq. (9) was approximately correct.

$$\overline{D_n} \approx f(\bar{F}_n, \bar{B}_n). \tag{10}$$

This relation was valid because

(i) approximately half the background was beam independent (i.e. cosmic rays, etc.) and thus was clearly independent of N_p.

(ii) The window was sufficiently narrow so that variation of the background number spectrum (B_n) with N_p could be kept small.

Since the efficiency E of the chamber did not depend upon N_p, eq. (5) could be used to calculate the spectrum-averaged quantities $\overline{P_n}$. The cross sections were then obtained by using an iteration procedure which averages eq. (6) over the ion chamber spectrum. (The ion chamber had a linear response to the number of protons per pulse.)

Before the equations were solved, the kill window had to be calibrated so that N_p could be computed from the beam current measurement. The neutron yield cross section $\sigma_{p,n}+\sigma_{p,pn}+2\sigma_{p,2n}+3\sigma_{p,3n}\ldots$ was measured by accepting all proton pulses, integrating the proton current and counting the total number of neutrons detected by the chamber S_n, where $S_n = S-S_b$ (S and S_b were the detected events for foil-in and foil-out runs, where S_b had been corrected for the beam dependence of the background).

Therefore, the neutron yield cross section was given by:

$$\sigma_{\text{neutron yield}} = \frac{S-S_b}{ENt\bar{N}_p}. \tag{11}$$

Eq. (11) held also for the data taken using the kill window. After the neutron yield cross section hasd been measured, $\bar{N}_p$ could be computed from the kill data. Once

TABLE 1

Summary of results [a])

E (MeV)	σ yield (mb)	σ(p, n) + (p, pn) (mb)	σ(p, 2n) (mb)	σ yield (mb)	σ(p, n) + (p, pn) (mb)	σ(p, 2n) (mb)
	Aluminium				Titanium	
7.0	38	38	-0.3 ± 1	341	341	
7.6	39	40	-0.6 ± 1	387	387	
8.0	53	55	-0.9 ± 1	428	428	
8.6	65	65	-0.1 ± 1	449	449	
9.0	73	72	0.6 ± 1	487	487	
9.4	77	77	-0.1 ± 1	513	513	
9.6	84					
10.0	82	82	0.1 ± 1	548	548	
10.4	86	87	-0.7 ± 1	531	531	
11.1	93	94	0.2 ± 1	570	570	
11.7	91			582	582	
12.0	97	96	0.7 ± 1	564	564	-4.3 ± 3
12.6	102	99	1.9 ± 1	569	572	-1.4 ± 2
13.3	105	105	-0.2 ± 1	567	557	3.2 ± 2
13.8	108	109	-0.4 ± 1	570	550	$10\ \pm2$
14.3	112	113	-0.7 ± 1	577	539	19.3 ± 4
14.6	113	114	-0.7 ± 1	603	536	$38\ \pm8$
15.0	112	112	-0.3 ± 1	564	525	$14\ \pm4$
	Cobalt				Zirconium	
7.0	433	433		177	177	-0.1 ± 1
7.6	466	466		258	258	
8.0	511	511		371	370	0.8 ± 1
8.6	494	494		481	462	$10\ \pm2$
9.0	518	518		577	568	6.2 ± 2
9.4	561	561		653	632	$11\ \pm2$
10.0	559	558	$1\ \pm0.5$	770	690	43
10.4	639	629	4.8 ± 1	906	714	96
11.1				946	805	106
11.7	630			1036		
12.0	592	569	6.5 ± 1	1021	639	187
12.6	689	622	32	1145	581	287
13.3	722	562	78	1223	591	325
13.8	688	500	93	1235	586	323
14.3	733	485	133	1311	557	377
14.6	752	452	149			
15.0	760	490	139	1237	579	329
	Vanadium				Silver	
7.0	532	532		244	243	-1.9 ± 2
7.3	533	533		260	260	
7.5				292	299	-5.5 ± 4
7.6	538	538		319	321	1.1 ± 1
7.8	550	550		305	305	
8.0	571	571		413	411	1.9 ± 1

[a]) All errors are $\pm10\,\%$ except where noted (standard deviations).

TABLE 1
(continued)

E (MeV)	σ yield (mb)	σ(p, n) +(p, pn) (mb)	σ(p, 2n) (mb)	σ yield (mb)	σ(p, n) +(p, pn) (mb)	σ(p, 2n) (mb)
8.7	607	607		526	509	7.2±1
9.0	629	629		574	540	17
9.4	644	644		659	578	41
10.0	694	694		823	624	95
10.4	664	670	−0.1±1	885	590	146
11.1	717			1104	626	257
11.7	734	729	2.5±1	1294	518	394
12.1	696	658	20	1289	414	445
12.6	800	661	76	1531	297	612
13.3	843	595	131	1767	270	747
13.8	884	502	200	1826	198	836
14.2	911	488	231	1870	209	855
14.7	903			1872		
15.0	885	397	236	1810	182	813
	Tantalum			Gold		
7.0	22±4	22± 4	−0.04±1	12±2	12± 2	0.2±1
7.3	31			21±4		
7.6	39	40	0.4 ±1	24±3	25± 3	−0.2±1
7.8				33		
8.0	62	62	0.1 ±1	42	42	0.2±1
8.7	132	98	17	90	83	3.6±1
9.0	185	101	42	114	95	9.6
9.4	265	113	76	169	126	21
10.0	451	124	163	278	148	65
10.4	552	108	220	343	142	100
11.1	834		417^{+40}_{-70}	577	112	232
11.7	1032			815	103	339
12.1	1105	56±20	523	878	102	384
12.3	1150			940		
12.6				1090		
13.3				1383	41± 8	671
13.8	1720	34±20	852	1560	82±16	725
14.2	1840			1650	15±15	820
14.7				1776		
15.0	1875	70±30	910	1811	113±30	866
			Niobium			
7.0	330	330	11.1	882	820	44
7.3	381	381	11.7	991	753	124
7.6	398	398	12.1	1032	702	167
8.0	487	484	0.1±1 12.6	1163	584	284
8.7	550	544	2.8±1 13.3	1376	392	500
9.0	621	621	13.8	1569	346	622
9.4	672	671	2.6±1 14.2	1640	273	694
10.0	756	733	5.8±1 15.0	1633	235	722
10.4	767	716	24			

$\overline{N_p}$ was known, the (p,n) and (p,2n) cross sections could be calculated. Therefore, at each energy the neutron yield cross section was measured and then the kill window was set to evaluate the (p, n) and (p, 2n) cross sections.

In the search for a (p, 3n) cross section, the data were analysed in a similar manner. The data analysis was programmed to be performed on an IBM 7094 computer.

9. Discussion of results

The results presented here were collected during two separate runs: one in June and the other in July, 1965. The results are summarized in table 1 and are displayed in figs. 6–13. Table 2 lists threshold energies for the (p, n), (p, pn), (p, 2n) and (p, 3n) reactions in the elements studied.

TABLE 2

Threshold energies

Isotope	Abundance (%)	Reaction threshold energy (MeV) (p, n)	(p, pn)	(p, 2n)	(p,3n)
$^{27}_{13}$Al	100	5.8	13.6		
$^{46}_{22}$Ti	7.9	8.0	13.5	22.6	
^{47}Ti	7.3	3.8	9.1		
^{48}Ti	73.9	4.9	11.9	15.6	
^{49}Ti	5.5	3.1	8.3	13.2	23.9
^{50}Ti	5.3	1.4	11.2	12.5	24.4
$^{51}_{23}$V	99.8	1.6	11.2	11.0	24.2
$^{59}_{27}$Co	100	1.9	10.7	11.0	23.2
$^{90}_{40}$Zr	51.5	6.9	11.9	16.6	
^{91}Zr	11.2	2.4	7.3	14.1	23.8
^{92}Zr	17.1	2.8	8.7	11.2	22.9
^{94}Zr	17.4	1.7	8.3	9.1	17.8
^{96}Zr	2.8	1.2	7.9	7.5	16.1
$^{93}_{41}$Nb	100	1.3	8.9	9.2	22.5
$^{107}_{47}$Ag	51.8	2.2	9.5	9.8	
^{109}Ag	48.2	0.9	6.7	8.3	18.8
$^{181}_{73}$Ta	100	0.9	7.6	7.7	
$^{197}_{79}$Au	100		8.1	8.2	

Since the detector could not distinguish between a (p, n) reaction and a (p, pn) process, only the sum of these reactions could be determined. However, in all of the mono-isotopic elements studied (V, Co, Nb, Ta and Au), the threshold for the (p, pn) reaction was quite close to that for the (p, 2n) reaction. In such cases it would be expected that the (p, 2n) reaction would dominate the cross section because of the Coulomb barrier preventing proton emission [3]). In addition, (p, pn) cross sections

have been measured in Co (refs. [3,14]), Ta (ref. [16])) and Nb (ref. [15])) and have been shown to be much smaller than those corresponding to the (p, n) process in the energy region of interest here. Therefore, in the elements listed above, the curves listed as (p, n)+(p, pn) could be taken as a good approximation of the (p, n) cross section.

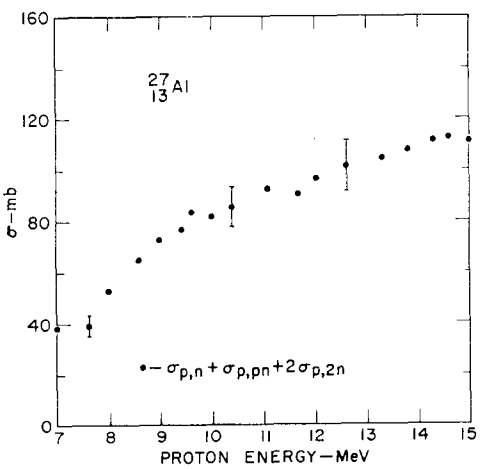

Fig. 6. Total neutron production cross section for aluminium.

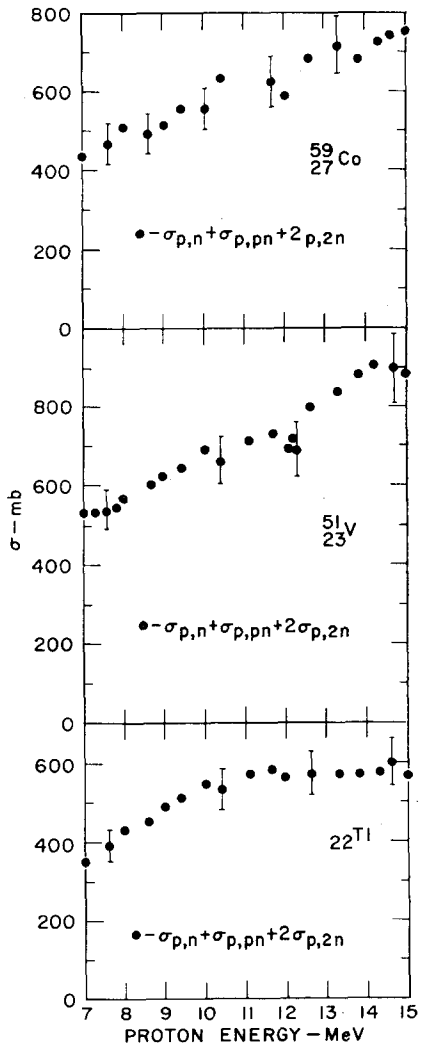

Fig. 7. Total neutron production cross sections for titanium, vanadium and cobalt.

The (p, 2n) reactions were found in all elements except aluminium. A general summary of the results follow in which values from other experimenters have been included, where available. Two graphs have been prepared for each element; the first displays the neutron yield cross section and the second, the (p, n) and (p, 2n) cross

sections. Typical standard deviations are plotted, and other experimenters' data have been designated A for activation analysis or N for neutron counting.

9.1. ALUMINIUM

Recently Bubb *et al.* [17]) have studied the reaction $^{27}Al(p, n)^{27}Si(A)$ and have found much structure evident in the excitation function. Some of their results are plotted in fig. 10 (accuracy ±10 %) and are in general agreement with ours around 7–8 MeV and fall somewhat below our values at 11 MeV. Since our target was rela-

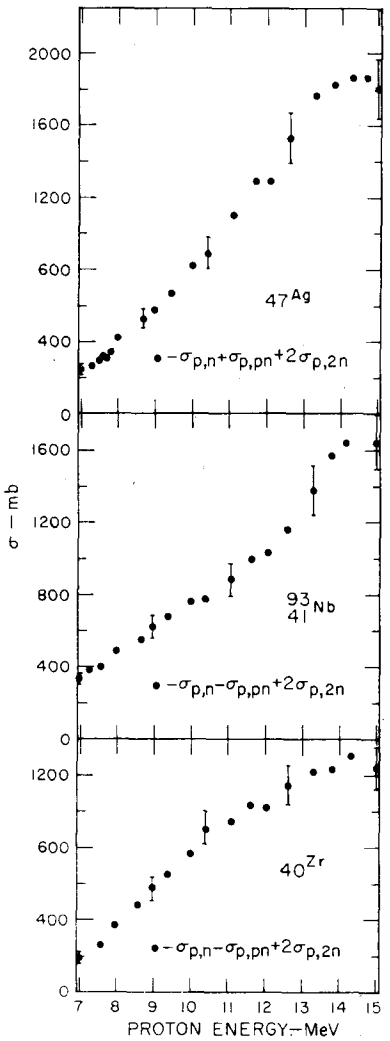

Fig. 8. Total neutron production cross sections for zirconium, niobium and silver.

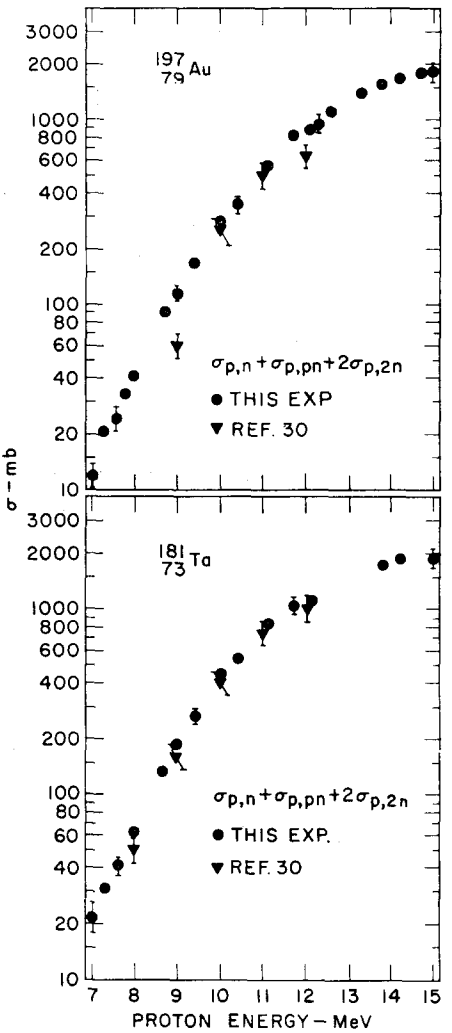

Fig. 9. Total neutron production cross sections for tantalum and gold.

tively thick, our cross-section values tend to be an average over a range of proton energies.

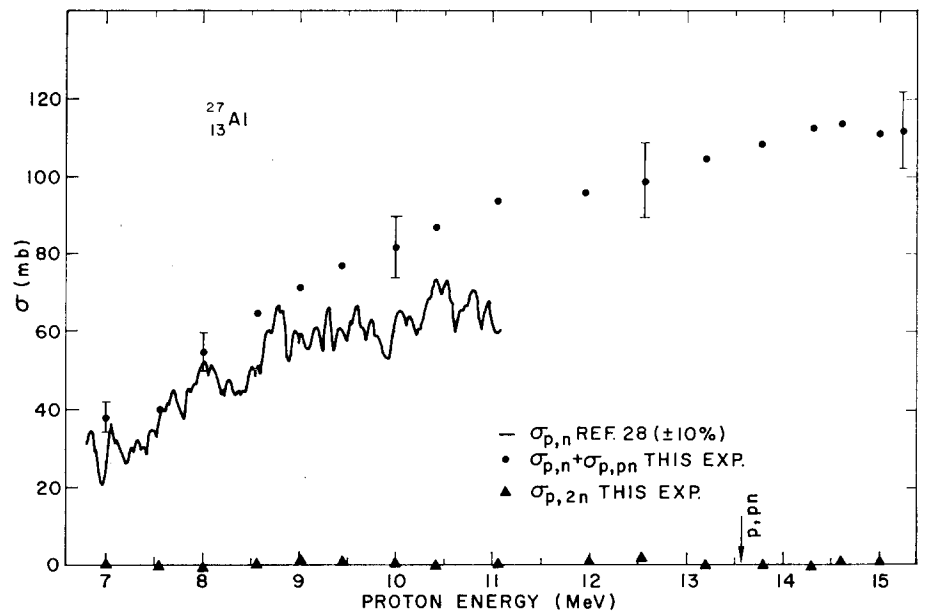

Fig. 10. The (p, n) and (p, 2n) cross sections for aluminium.

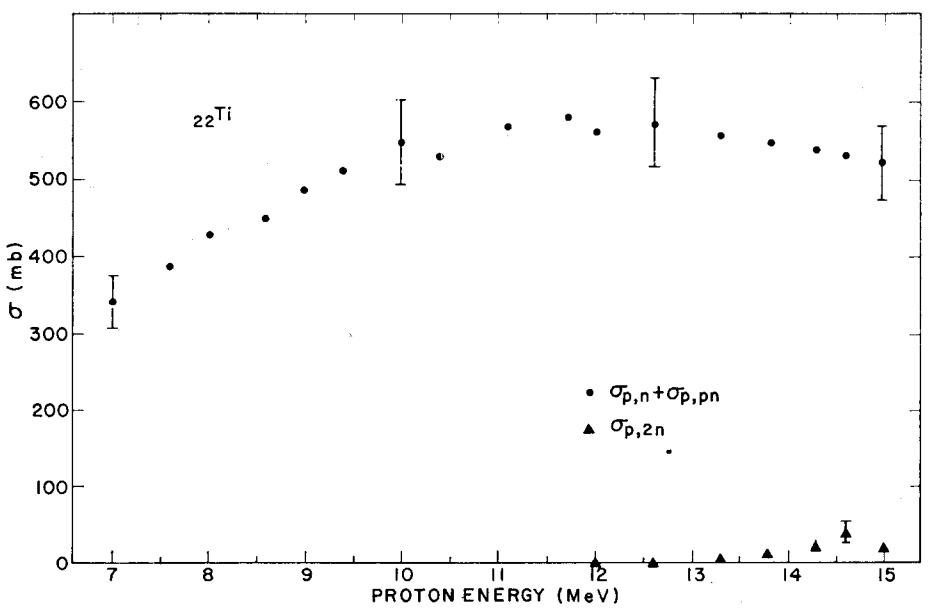

Fig. 11. The (p, n) and (p, 2n) cross sections for titanium.

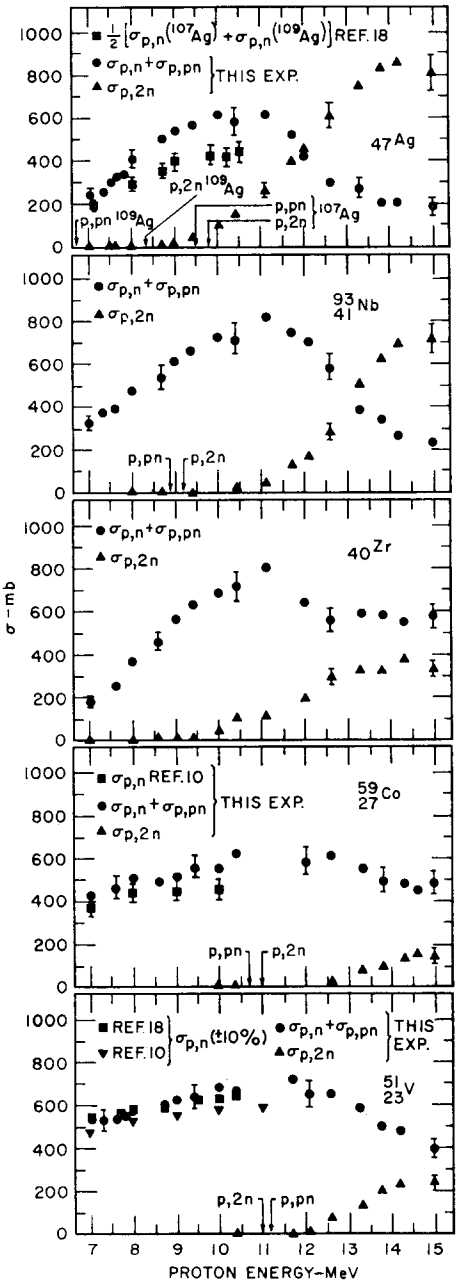

Fig. 12. The (p, n) and (p, 2n) cross sections for vanadium, cobalt, zirconium, niobium and silver.

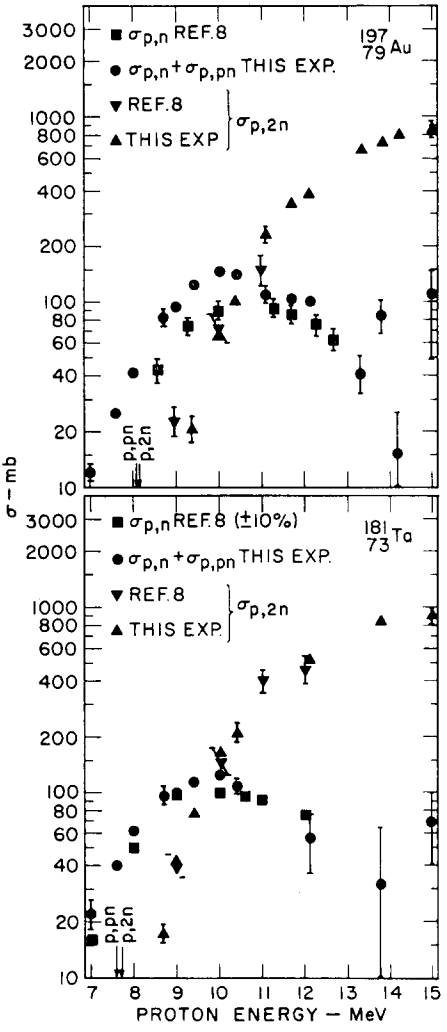

Fig. 13. The (p, n) and (p, 2n) cross sections for tantalum and gold.

9.2. TITANIUM

No other data are available on an elemental target; values for all of the isotopes are not available.

9.3. VANADIUM

The (p, n) data from Wing and Huizenga [18])(A) and from Hansen and Albert [10]) (N) have been included. Our data agree quite well with those of Wing *et al.* and are slightly higher ($\approx 10\,\%$) than those of Hansen and Albert.

9.4. COBALT

The (p, n) data from Hansen and Albert [10])(N) have been included. As in the case of vanadium, our results are 10–15 % higher than their values.

9.5. ZIRCONIUM

No other data are available on an elemental target; values for all of the isotopes are not available.

9.6. NIOBIUM

James [15]) and Forsthoff *et al.* [19]) have reported the excitation function for the reaction ^{93}Nb(p, n)^{93m}Mo(A). From our results and James' values of 60 mb at 10 MeV and 250 mb at 15 MeV, we surmise that up to 13 or 14 MeV the reaction proceeds directly to the ground state most of the time. The Q-values for production of both the ground state and excited state isomers have been observed at 1.3 and 2.7 MeV, respectively [20–22]). However, only the excited state reaction can be studied by activation analysis since its half-life is 7 h compared to the half-life of the ground state of $\approx 10^4$ y.

9.7. SILVER

The (p, n) cross sections for ^{107}Ag and ^{109}Ag have been measured by Wing and Huizenga [18])(A). The average of these two excitation functions has been plotted with our data on fig. 12. At 10 MeV, their values are 30 % lower than ours. However, the (p, pn) thresholds in ^{109}Ag is 6.7 MeV compared to a (p, 2n) threshold of 8.3 MeV. Cohen [3]) has shown that the (p, pn) reaction should dominate over the (p, 2n) process if the (p, pn) threshold is much lower than the (p, 2n) threshold. Therefore, we might expect a large (p, pn) reaction in ^{109}Ag. In ^{107}Ag the two thresholds are only 0.3 MeV apart, and the (p, pn) cross section has been measured and shown to be quite small (around 10 mb at 15 MeV).

If we postulate that the difference in the two excitation functions is due to a (p, pn) contribution from ^{109}Ag, we can give a rough estimate of the magnitude of that contribution. (See table 3.)

9.8. TANTALUM

Tantalum has been studied previously by Hansen *et al.* [8]), who measured (p, n) (A) and (p, 2n)(N) cross sections with proton energies up to 12 MeV. Our data agree favourably with theirs. Also, Holbrow and Barschall [23]) have measured the neutron yield cross section for Ta(N), and their results are in good agreement with ours.

9.9. GOLD

Holbrow and Barschall [23]) measured the neutron yield cross section for gold. Agreement at 10 and 11 MeV is good, but their 9 and 12 MeV points fall below our curve. Hansen *et al.* [8]) measured the (p, n)(A) and the (p, 2n)(N) cross sections in gold. Their (p, 2n) values are in general agreement with ours, but their (p, n) values fall about 30 % below our curve.

The study of the (p, n) reaction by activation analysis in gold is very difficult because of the complex decay schemes of the two isomers of ^{197}Hg which are produced. The technique used by the above authors was to measure the partial cross section for each isomer and then add the resulting values. Both 24 h and 65 h activities are pro-

TABLE 3

(p, pn) cross sections in ^{109}Ag

Proton energy (MeV)	σ(p, pn) (mb)
7.5	120± 80
8.5	240±120
9.5	280±140
10.5	320±150

duced; the 24 h isomer is easily handled since only a single gamma line (133 keV) is involved, and its conversion coefficient is known. However, the 24 h isomer decays to the ground state, which is also produced by the reaction. The ground state decays by electron capture to a 77 keV level in ^{197}Au. The K-capture X-rays from ^{197}Hg and the 77 keV gammas were not resolved in this experiment. Thus the spectrum is very complicated, and the analysis rests on knowing the K-capture fraction C_K of ^{197}Hg and the internal conversion coefficient of the 77 keV gamma. The former parameter was calculated from the decay energy, and the latter has been experimentally measured. Low values of the cross section would result if C_K were overestimated or if the value for the internal conversion coefficient was too low. The uncertainty in these parameters is probably the cause of the discrepancy between the two excitation functions, since the values by the same authors on tantalum are in good agreement with our results. (An overestimate of C_K by 40 % would be required to bring the two excitation functions into agreement; a much larger increase in the internal conversion coefficient would be required, since the cross section is relatively insensitive to that parameter.)

10. Error analysis

The following were the main sources of error in this experiment:

(i) Drifts and instabilities of the beam monitoring-system Faraday cup, micro-microammeter and current integrator. The small average current normally used (10 pA) made the system very sensitive to cable noise and leakage currents across insulators. An error of $\pm$ 5 % was derived from the repeatability and consistency of our data.

(ii) Non-uniformities of the thin foils used as targets. As mentioned previously, foil thicknesses were checked with an alpha source and a silicon-barrier detector. All of the foils except those of Co and Nb were found to be uniform to $\pm$5 % or better; the Co foil to $\pm$7 % and the Nb foil to $\pm$10 %. However, since the beam size was about 0.6 by 1.3 cm, many of these irregularites were undoubtedly averaged out.

(iii) Fluctuations in the background caused mainly by short-lived activities produced in the target foils as well as on collimators, the ion chamber foils and the beam stop. Since the background was checked constantly, the errors added here were only $\pm$2 to 3 %.

(iv) Drifts in the electronics and hence in the chamber efficiency as well as a basic uncertainty in the chamber efficiency. These occurred because no correction was made for the incident neutron energy.

The average energy of the fission neutrons from ^{252}Cf is said [12]) to be around 2.2 MeV. Also, the average energy of neutrons emitted from (p, n) and (p, 2n) processes (in the medium and heavy elements) is expected to be in the 1–4 MeV range [24, 25]). Since a Monte Carlo calculation showed a slight efficiency dependence on energy for a detector quite similar to the one used here [12]), it was concluded that this effect was not too important. Although the chamber efficiency was measured during the cyclotron runs and was repeatable to $\pm$2 %, it was considered accurate only to $\pm$3 to 4 %.

(v) Statistical sources due to counting. In general, these were kept small because a typical data point involved at least 100000 gates in which, on the average, 40000 to 100000 neutrons would be detected. Signal-to-noise ratios ran typically from 5 : 1 to 10 : 1. Errors were estimated by using a computer code which generated counting statistics and calculated uncertainties in the final results. From this analysis an error of $\pm$2 to 3 % was added.

In addition to the above, the proton energy was considered accurate to $\pm$0.100 MeV. (It was measured by the standard method of determining its range in aluminium.)

By virtue of the errors assigned above, the neutron yield cross sections were considered accurate to $\pm$10 % (standard deviations). The (p, n) and (p, 2n) cross sections were also considered accurate to $\pm$10 % except in regions where one of the cross sections is very much smaller than the other. However, the ratios of the (p, 2n) cross sections (to the sum of the (p, n)+(p, pn) plus the (p, 2n) cross sections) used to calculate the level density parameter a should be more accurate since most of the above

effects cancel out of the equation for the ratio. These numbers were considered good to ±5%.

11. Level-density parameters

Following Blatt and Weisskopf [26]) the level-density parameter a can be calculated if both the (p, n)+(p, pn) and the (p, 2n) cross sections are known. Assuming that the cross section for the inverse reaction is constant, we have

$$\frac{\sigma_{p,2n}}{\sigma_{p,n}+\sigma_{p,pn}+\sigma_{p,2n}} = \frac{\int_0^{T_p-E_{2n}} e_n w(U)\mathrm{d}e_n}{\int_{T_p-E_{2n}}^{T_p-E_{1n}} e_n w(U)\mathrm{d}e_n + \int_0^{T_p-E_{2n}} e_n w(U)\mathrm{d}e_n}, \tag{12}$$

where T_p is the proton kinetic energy in the centre-of-mass system, E_{1n} the (p, n) threshold, E_{2n} the (p, 2n) threshold, e_n the energy of the emitted neutron and $w(U) = w(u-\delta)$ = the level density function proportional to

$$\frac{\exp\left(2[a(u-\delta)]^{\frac{1}{2}}\right)}{(u-\delta)^2},$$

where $u = T_p - E_{1n} - e_n$, a is the level-density parameter and δ the pairing energy (from Cameron [27]). Eq. (12) also assumes that a statistical model is valid and that the probability of gamma-ray and proton emission is small compared to that for neutron emission; an assumption which may not be justified in general. However, eq. (12) is used here to facilitate comparison with previous measurements of (γ, n) and (γ, 2n) cross section ratios by Bramblett *et al.* [25, 30]). The same formula was employed by these authors in their analysis. No attempt is made here to extend the theory.

The above ratio was calculated from the mono-isotopic data and was evaluated at all proton energies. Then, for each isotope, eq. (12) was evaluated at various energies, and a familty of curves was produced using a as the parameter. The value of a defining the curve which best fit the experimental data was thus determined. The fit to the experimental data was good at proton energies more than 2–3 MeV above the (p, 2n) threshold, but below this point the calculated curve overestimated the experimentally measured ratio (see fig. 14). The values of a are plotted in fig. 15. Drawing the best straight line through these points yielded $a = \frac{1}{25}A$.

It is of some interest to compare the a values obtained in the present work with those given by previous authors, even though it should be recognized that all of the comparisons are not equally valid. The a-values obtained in the present work are in good agreement with those of Dostrovsky *et al.* [24]) which were derived from their study of nuclear evaporation processes between $A = 46$ and $A = 70$. The best fit to the data considered in that reference is for an a-value of $\frac{1}{20}A$, although the criteria used for finding the "best fit" are somewhat vague (see fig. 4 of ref. [24])). More recently, several other analyses of nuclear reaction data have yielded larger values of the

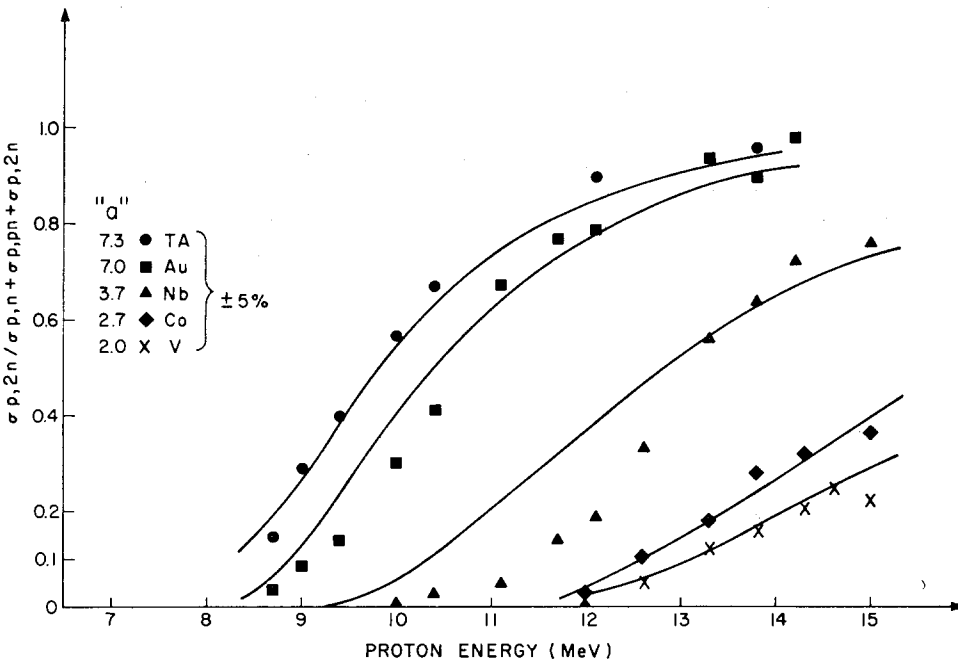

Fig. 14. Comparison of the ratio $\sigma(p, 2n)/\sigma(p, n)+\sigma(p, pn)+\sigma(p, 2n)$ with the theoretical expression given in eq. (12).

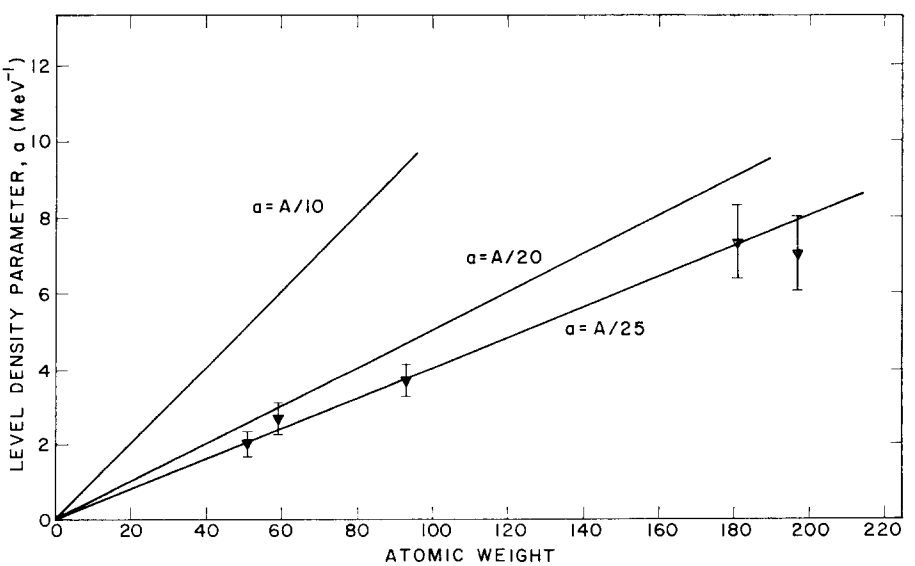

Fig. 15. Level density parameter a as a function of atomic weight. It can be seen that the best fit is for the case where $a = {}^{1}/_{25}A$.

level-density parameter. Wong *et al.* [28]) give a value of approximately $\frac{1}{8}A$ from their studies of neutron spectra from (p, n) reactions. Lang [29]) found a best value of $\frac{1}{10}A$ by analysing data from heavy-ion reactions as well as (p, α), (p, α', γ), (α, α') and (n, p) results. It is easy to see that there is no convincing agreement among the a-values obtained in the present work with those quoted by previous authors. The reason for this confusing state of affairs probably lies in the rather crude statistical assumptions used to obtain the level of density function $w(u)$. It is probably too much to expect that this model should yield really quantitative agreement for the many different types of reactions and nuclides considered in the references of previous work.

An attempt to make a more meaningful comparison was made by searching for reactions which are similar to the ones considered in the present work. Bramblett *et al.* [25, 30]) have measured the (γ, n) and (γ, 2n) cross sections for a number of elements, using experimental methods roughly similar to the ones reported here. In several cases, (Ta and Au for example) they bombarded the same target materials. They also followed exactly the same procedure in calculating a from the ratio of the (γ, n) and (γ, 2n) cross sections and employed the same form of the level density function $w(U)$. However, they did not include the pairing energy δ in their calculations. It was found that the a-value was not a strong function of the pairing energy by recalculating the a-values using the level-density function without the pairing energy and obtaining approximately the same value of a ($\frac{1}{25}A$). Bramblett *et al.* [25, 30]) find a best value for a of roughly $\frac{1}{10}A$ from their data. This is a factor of two larger than the value obtained in the present work. It seems, therefore, that when the compound nucleus is formed by gamma rays, more channels are available for neutron decay than when it is formed by protons. A possible explanation of this result is that the gamma-ray reactions proceed almost entirely by a compound nucleus process so that the decay is independent of the formation and all levels of the residual nucleus can contribute. On the other hand, the reactions induced by charged particles are more likely to proceed by a direct, one-step process which would mean that the number of final states may be more restricted. A more direct comparison with gamma-ray induced reactions would be to observe the (γ, n), (γ, 2n) and (p, n), (p, 2n) reactions for the same residual nucleus. No data for such a comparison are available at the present time.

The authors would like to thank all the people at LRL-Livermore who made this experiment possible; in the mechanical shop, V. Gregory and G. Clough and all their crew; in the electronic shop, C. Sewell and D. Moyer, as well as all the other technicians; also, M. Williamson and A. Van Lehn, who prepared the foils and T. Harper, who assisted during the cyclotron runs and also helped analyse the data. Finally, we would like to give special thanks to D. Rawles and all the cyclotron operators, without whose cooperation and assistance this experiment would never have succeeded.

References

1) J. R. Grover and R. J. Nagle, Phys. Rev. **134** (1964) B1248
2) C. G. Andre *et al.*, Phys. Rev. **101** (1956) 645
3) B. L. Cohen and E. Newman, Phys. Rev. **99** (1955) 718;
   B. L. Cohen, E. Newman and T. H. Handley, Phys. Rev. **99** (1955) 723
4) H. A. Tewes, Phys. Rev. **98** (1955) 25
5) J. W. Meadows, Phys. Rev. **91** (1953) 885
6) S. N. Ghoshal, Phys. Rev. **80** (1950) 939
7) N. T. Porile *et al.*, Nuclear Physics **43** (1962) 500
8) L. F. Hansen, R. C. Jopson, H. Mark and C. D. Swift, Nuclear Physics **30** (1961) 389
9) J. Olkowsky, I. Gratot and M. Le Pape, Nuclear Physics **24** (1960) 84
10) L. F. Hansen and R. D. Albert, Phys. Rev. **128** (1962) 291
11) D. S. Mather, P. Fieldhouse and A. Moat, Phys. Rev. **133** (1964) B1403;
    B. C. Diven, H. C. Martin, R. F. Taschek and J. Terrell, Phys. Rev. **101** (1956) 1012;
    D. A. Hicks, J. Ise and R. V. Pyle, Phys. Rev. **101** (1956) 1016;
    F. Reines, C. L. Cowan, Jr., F. B. Harrison and D.S. Carter, Rev. Sci. Instr. **25** (1954) 1061
12) V. J. Ashby, C. H. Catron, L. L. Newkirk and C. J. Taylor, Phys. Rev. **111** (1958) 616
13) H. H. Selinger, C. A. Ziegler and I. Jaffe, Phys. Rev. **101** (1956) 998
14) R. A. Sharp, R. M. Diamond and G. Wilkinson, Phys. Rev. **101** (1955) 1493
15) R. A. James, Phys. Rev. **93** (1953) 288
16) B. L. Cohen, E. Newman, R. A. Charpie and T. H. Handley, Phys. Rev. **94** (1953) 620
17) I. F. Bubb, J. M. Poate and R. H. Spear, Nuclear Physics **65** (1965) 655
18) J. Wing and J. R. Huizenga, Phys. Rev. **128** (1962) 280
19) C. W. Forsthoff, R. H. Goeckermann and R. A. Naumann, Phys. Rev. **90** (1953) 1004
20) C. H. Johnson, A. Galonsky and J. P. Ulrich, Bull. Am. Phys. Soc. **2** (1957) 177D2
21) C. H. Johnson and A. Galonsky, Bull. Am. Phys. Soc. **5** (1960) 443C13
22) R. Patterson, Phys. Rev. **95** (1954) 303A
23) C. H. Holbrow and H. H. Barschall, Nuclear Physics **42** (1963) 264
24) I. Dostrovsky, Z. Fraenkel and G. Friedlander, Phys. Rev. **116** (1959) 683
25) R. L. Bramblett, private communication
26) J. M. Blatt and V. F. Weisskopf, Theoretical nuclear physics (John Wiley and Sons, New York, 1952)
27) A. G. W. Cameron, Can. J. Phys. **36** (1958) 1040
28) C. Wong, J. D. Anderson, J. W. McClure and B. D. Walker, Nuclear Physics **57** (1964) 515
29) D. W. Lang, Nuclear Physics **26** (1961) 434 (A/10)
30) R. L. Bramblett, J. T. Caldwell, G. F. Auchampaugh and S. C. Fultz, Phys. Rev. **129** (1963) 2723;
    R. L. Bramblett, J. T. Caldwell, R. R. Harvey and S. C. Fultz, Phys. Rev. **133** (1964) B869;
    S. C. Fultz, R. L. Bramblett, J. T. Caldwell and R. R. Harvey, Phys. Rev. **133** (1964) B1149